Exp Fluids (2009) 46:309–322
DOI 10.1007/s00348-008-0561-x

RESEARCH ARTICLE

An experimental study of the liquid film on a vertical wire under the action of an impinging annular jet

Simone Zuccher

Received: 22 February 2008 / Revised: 26 August 2008 / Accepted: 27 August 2008 / Published online: 20 September 2008

Abstract The liquid film remaining on a wire withdrawn from a liquid bath and forced through an annular jet is experimentally investigated on a dedicated facility. An optical laser-based technique recently introduced to study liquid-film instabilities on small-radius cylinders allows the measurement of the mean final thickness and wave characteristics. Experimental results are compared to analytical predictions obtained with a simple model specifically derived for this configuration and based on liquid-film properties (density, viscosity and surface tension) and operating parameters (wire speed, nozzle dimensions and stagnation pressure). Such a model relies on the knowledge of pressure-gradient and wall shear-stress distributions generated by the annular jet radially impinging on the cylinder. Different correlations providing the maxima of these profiles are employed and, after some improvements to the original "knife" model, the mean final thickness is correctly predicted. Successful results are obtained, also, using a simple expression derived from the LLD theory. The experimental measurement of surface-perturbation features (wave amplitude, wavelength and amplification factor) as a function of the operating parameters leads to some important conclusions that could have a remarkable and direct influence on the industrial process of wire coating.

S. Zuccher
Environmental and Applied Fluid Dynamics Department,
von Kármán Institute for Fluid Dynamics,
72 Chausse de Waterloo, 1640 Rhode-Saint-Genèse, Belgium

Present Address:
S. Zuccher (✉)
University of Verona, Ca' Vignal 2, Strada Le Grazie 15,
37134 Verona, Italy
e-mail: zuccher@sci.univr.it

1 Introduction

The deposition of a thin liquid film on a solid surface is the basis of numerous coating techniques used in industrial processes such as paper and photographic film manufacturing, finishing of steel strips, and wire coating. Here we focus on the last process which, more generally, aims at covering a small-radius cylinder with a thin layer of another material, initially liquid, so as to protect or paint textile fibers, optical fibers, electric wires, etc. (Tadmor and Gogos 1979). In the commonly used dip-coating method, the coating material is applied by withdrawing the wire from a liquid bath and by letting it dry without undergoing any other kind of treatment. The mean final thickness h_f depends on the wire radius R, fluid density ρ, surface tension σ, dynamic viscosity μ, and wire velocity U (for a detailed review on the subject of fiber coating the reader is referred to Quéré (1999) and literature cited therein). Since the wire radius and the coating properties are fixed, the desired final thickness h_f is achieved by controlling U. The high productivity required in industrial processes, however, imposes high speeds that result in an increase of the coating thickness. In order to combine high productivity and precisely controlled film thickness, more complex coating techniques have been devised. The excess (extra) liquid material is removed by a mechanical or hydrodynamic process known as doctoring. Die coating, for which (doctor) blades or special dies are employed, is a mechanical technique whereas gas-jet wiping, which uses a blast of air to wipe off the undesired liquid, is hydrodynamic. Since die coating involves a direct

physical contact between the liquid and the mechanical device (the die), in many practical cases—especially those involving very high temperatures—the only feasible alternative is annular jet wiping (see Fig. 1a for a sketch of the technique). Jet finishing, jet stripping, or gas jet wiping are all synonyms used to identify the same process in which the thickness of a liquid coating is controlled by the stripping action of a gas jet.

Despite the importance of such a technique for industrial applications, experimental or numerical data specifically regarding annular jet wiping configurations have never been published. The only available results, to the author's knowledge, reduce to very few experiments carried out at the von Kármán Institute for Fluid Dynamics over the last few years (Anthoine 1996; Zuccher 1999).

Contrary to the wire-coating configuration, jet wiping has been extensively studied in the planar case. Thorton and Graff (1976) proposed a theoretical coating-weight model based on the maximum flux theory for jet stripping, in which the gravity force is supplemented by a pressure gradient originating from the jet. In such seminal work the effect of the wall shear stress induced by the stripping jet was ignored. Tuck (1983) considered a similar approach and analyzed the stability of the solutions for long-wavelength perturbations. Ellen and Tu (1984, 1985), Tu (1995), and Tu and Wood (1996) refined the work of Thorton and Graff (1976) by introducing the wall shear stress on the surface of the liquid coating due to the wiping jet and obtained a better agreement with industrial coating weight data. Lacanette et al. (2005a, b) considered the more detailed, but numerically demanding, approach involving direct numerical simulation of the gas-jet wiping in the continuous galvanizing process, whereas Naphade et al. (2005) employed a finite-volume commercial code to compute the pressure and wall shear stress profiles required by the model to predict the coating weight as a function of different operating parameters. Lacanette et al. (2006) analyzed the jet-wiping mechanism by comparing for the first time a 1D lubrication analytical model, 2D VOF-LES simulations and experimental results, demonstrating the complementarity of the three approaches and showing a good agreement between them. Elsaadawy et al. (2007) developed an air-knife wiping model for the liquid zinc coating in the continuous hot dip galvanizing process based on improved correlations for pressure and wall shear stress obtained by a combination of experimental and computation techniques. Gosset and Buchlin (2007) carried out an analysis of the gas-jet wiping process in hot-dip galvanization considering also the occurrence of a violent film instability, better known as splashing, which limits the applicability of the wiping technique.

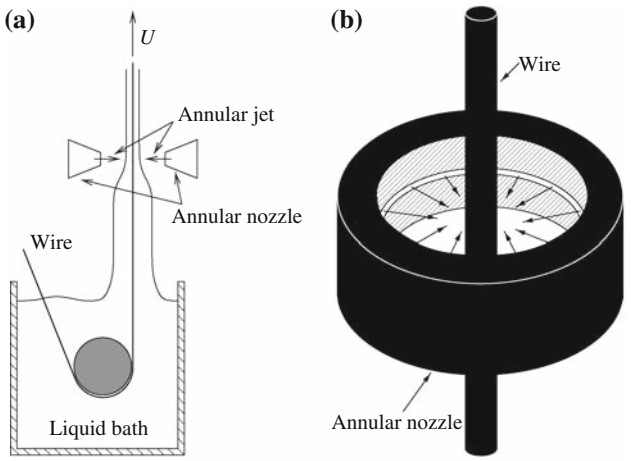

Fig. 1 **a** Annular jet wiping in the wire coating process. A thin liquid layer is formed on the surface of a wire withdrawn from a liquid bath. The mean final thickness h_f is controlled by operating conditions such as nozzle geometry and pressure, stripping velocity, etc. **b** Annular nozzle and annular jet surrounding a small cylinder set in the center (note that the geometrical dimensions are not respected in the figure)

The development of a reasonable coating model depends on the knowledge of pressure gradient and wall shear stress distributions on the impinging surface and due to the jet action. In the wire coating process, an annular jet radially impinges on a small tube in the inward direction, as shown in Fig. 1b. It should be noted that "annular" here refers to the fact that the nozzle surrounds the wire in an annular fashion and not to other jet configurations normally referred to as annular (for the latter, which are completely different from the present one, see, e.g., Del Taglia et al. 2004; Chen et al. 2003; Patte-Rouland et al. 2001). Data regarding the configuration reported in Fig. 1b cannot be found in published literature. On the other hand, many studies in other configurations have been carried out in recent years from both numerical and experimental viewpoints. Most of them refer to the use of an impinging jet for cooling purpose (Pavlova and Amitay 2006), while in the present work the jet is used exclusively to reduce the final thickness of the liquid film on the wire. For an account of studies and correlations of pressure and wall shear stress distributions of impinging jets on flat plates or cylinders the reader is referred to Zuckerman and Lior (2005). The recent work by Esirgemez et al. (2007) is an experimental study of a round jet impinging on a convex cylinder, while Nada (2006) considered single and multiple jets impinging on a cylinder in different jets-cylinder configurations, but excluded the one in Fig. 1b. Other classical works referring to cylindrical geometries, but still different from the one shown in Fig. 1b, are Chan et al. (2002) and Olsson et al. (2005). For recent studies of jets impinging on a flat plate and, thus, possible suggestions on how to treat the annular jet under investigation, the reader is referred to the following works and references therein: Zuckerman and

Lior (2007); Silverman et al. (2006); Ashforth-Frost and Rüdel (2002); Maurel and Solliec (2001); Phares et al. (2000a, b).

Measurement techniques for detecting liquid-film thickness encompass film conductance and film capacitance methods, the needle contact method, the light absorption method, the fluorescence method, the γ-ray and X-ray absorption methods (Hewitt 1978; Alekseenko et al. 1994). Mouza et al. (2000) developed a photometric technique based on the absorption of light passing through a layer of dyed liquid; Stelter et al. (2000) presented an optical method suitable for the characterization of the behavior of viscoelastic polymer solutions in elongational flows, and, earlier, Nozhat (1997) applied a laser interferometry technique to measure the thickness of the liquid flowing on the inner surface of a glass tube. More recently, Zuccher (2005) introduced a laser-based measurement method that allows the detection of both mean final thickness and perturbations of the liquid film. This technique has been successfully employed to characterize the film instabilities occurring during the die-coating process of wires (Zuccher 2008).

If such perturbations are stable but feature large amplitudes or, in the worst-case scenario, are unstable with increasing-in-time/space amplitudes, the final coating can be severely compromised. In these cases, the industrial product is unacceptable either because typical values of the coating characteristics become unknown and, thus, uncontrolled (e.g. the heat-transfer coefficient, which is important in chemical reactions, varies depending on the local coating thickness) or because the final finish may not be aesthetically good enough. Since the instabilities can set a limit on the production rate or dictate the selection of the liquid in precision coating, experimental investigations are of considerable practical significance.

Due to the complete lack of literature and data on configurations that could be used for the understanding of the annular-jet wire-coating process, this work aims at providing some experimental measurements of the mean final thickness and characteristics of the perturbations as a function of the operating parameters.

2 Modelling of annular jet wiping for the prediction of the mean final thickness

With the final goal of deriving a simple model to predict h_f, let us focus on the liquid film and consider the Navier–Stokes equations in cylindrical coordinates under the following assumptions: (1) the axial velocity component is much larger than the radial one which is, thus, negligible; (2) the flow is axisymmetric; (3) inertial forces are negligible compared to viscous stresses (lubrication approach); (4) the liquid film is stationary; (5) the static pressure is constant through the liquid film in the direction normal to the wire surface; (6) the jet is not affected by the coating, i.e. pressure and shear stress distributions are the same with or without the film (this is confirmed by Lacanette et al. (2006) for the planar case). Under such assumptions, the axial-momentum equation reduces to

$$\frac{\mu}{r}\frac{\partial}{\partial r}\left(r\frac{\partial u(x,r)}{\partial r}\right)=\frac{\mathrm{d}p(x)}{\mathrm{d}x}+\rho g-\sigma\frac{\mathrm{d}^3h(x)}{\mathrm{d}x^3}, \tag{1}$$

where x and r are the axial and radial coordinates as shown in Fig. 2; μ and ρ are, respectively, the viscosity and density of the liquid coating; $p(x)$ is the pressure profile which depends only on x; $u(x, r)$ is the longitudinal (axial) velocity component, g is the gravity acceleration and $h(x)$ is the liquid-film thickness. The effect of the liquid surface tension can be neglected in a first-approximation model (as done, for instance, by Ellen and Tu 1985) owing also to the recent conclusions of Gosset and Buchlin (2007), who proved that σ does not play a significant role in typical planar jet-wiping configurations. Since the pressure within the liquid film is assumed constant at fixed x and the surface tension disregarded, it can be concluded that $\mathrm{d}p(x)/\mathrm{d}x = \mathrm{d}p(x)_{\mathrm{jet}}/\mathrm{d}x$, where $p(x)_{\mathrm{jet}}$ is the pressure distribution of the jet impinging on the wire and it is generally approximated by a Gaussian distribution as in Fig. 3.

Equation (1) is supplemented by the boundary conditions

$$\begin{aligned} &u(x,r)=U \quad \text{at} \quad r=R \\ &\mu\frac{\partial u(x,r)}{\partial r}=\tau_{\mathrm{jet}}(x) \quad \text{at} \quad r=R+h(x)=H(x), \end{aligned} \tag{2}$$

where U is the wire velocity, $\tau_{\mathrm{jet}}(x)$ is the shear-stress profile due to the jet impinging on the wire with a typical shape as in Fig. 3, and R is the wire radius. Since $\mathrm{d}p(x)/\mathrm{d}x = \mathrm{d}p(x)_{\mathrm{jet}}/\mathrm{d}x$ and $\tau_{\mathrm{jet}}(x)$ cannot be confused with other notations, $\mathrm{d}p(x)_{\mathrm{jet}}/\mathrm{d}x$ and $\tau_{\mathrm{jet}}(x)$ will be denoted simply as $\mathrm{d}p(x)/\mathrm{d}x$ and $\tau(x)$.

The velocity profile of the liquid film as a function of x and r can be obtained by integrating equation (1) subject to boundary conditions (2),

$$u(x,r)=U+\frac{A}{4}(r^2-R^2)+H\left(B-\frac{A}{2}H\right)\ln\left(\frac{r}{R}\right), \tag{3}$$

with A and B functions of x and defined as

$$\begin{aligned} A(x)&=\frac{1}{\mu}\left(\frac{\mathrm{d}p(x)}{\mathrm{d}x}+\rho g\right) \\ B(x)&=\frac{\tau(x)}{\mu}. \end{aligned} \tag{4}$$

Once the velocity profile is known, the volumetric liquid flow rate $Q=\int_R^{H(x)}2\pi r u(x,r)\mathrm{d}r$ is computed as

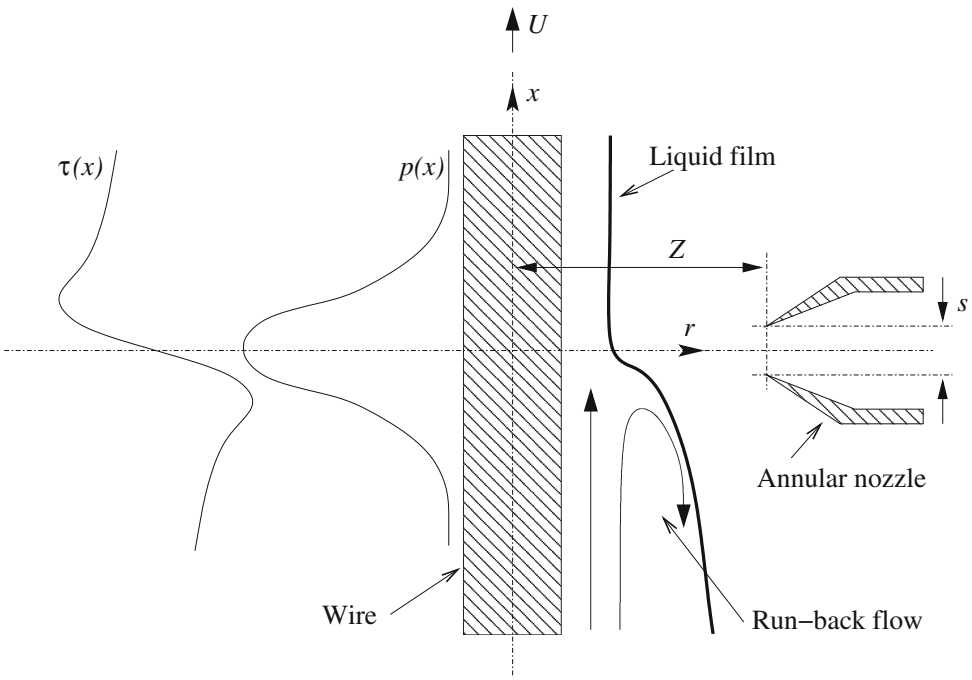

Fig. 2 Schematic diagram of the annular-jet stripping process. The geometry is axial-symmetric and it is shown on the *right side* of the figure. The pressure and wall shear stress distributions generated by the jet impinging on the wire are reported on the *left side*. (Geometrical dimensions are not respected in the figure)

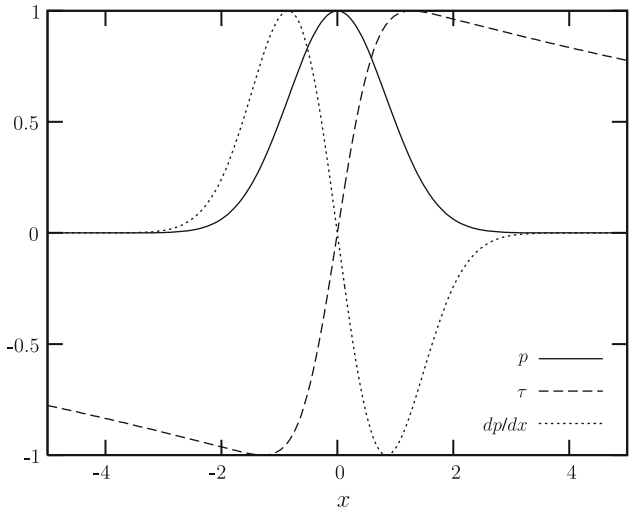

Fig. 3 Normalized profiles of jet pressure p, shear stress τ and pressure gradient $\mathrm{d}p/\mathrm{d}x$ as a function of x with $p = p(x)/\max(p) = \exp(\log(1/2)x^2)$ and $\tau = \tau(x)/\max(\tau) = (\mathrm{erf}(1.4x) - \mathrm{atan}(x/10)2/\pi)/0.908$)

$$Q\left(H, \frac{\mathrm{d}p}{\mathrm{d}x}, \tau\right) = 2\pi\left[\frac{U}{2}(H^2 - R^2) + \frac{A}{16}(H^2 - R^2)^2 + C\left[\frac{R^2}{4} + \frac{H^2}{4}\left(2\ln\left(\frac{H}{R}\right) - 1\right)\right]\right],$$

where $C = H[B - HA/2]$.

Q depends on x through $H(x) = h(x) + R$, $\mathrm{d}p(x)/\mathrm{d}x$ and $\tau(x)$. However, if $p(x)$ and $\tau(x)$ are available as empirical correlations from experimental or numerical investigations (see, e.g., Fig. 3), the equation above expresses a constraint between two unknowns, Q and H, at a fixed position x. Therefore, Q remains a function of two *independent* variables H and x,

$$Q(H,x) = 2\pi\left[\frac{U}{2}(H^2 - R^2) + \frac{A(x)}{16}(H^2 - R^2)^2 + C(x)\left[\frac{R^2}{4} + \frac{H^2}{4}\left(2\ln\left(\frac{H}{R}\right) - 1\right)\right]\right], \quad (5)$$

where H is independent of x in the sense that so far it is still an unknown function of x. Practically, $H(x)$ is derived from (5) simply as the level curve (contour line) of function $Q(H, x)$ at a fixed level $\bar{Q}$ of the flow rate. This is consistent with the fact that in stationary conditions Q must be constant, i.e. the continuity equation has to be satisfied. Mathematically, equation (5) is not sufficient to determine both $Q(x) = \bar{Q}$ and $H(x)$. However, from physical considerations, the flow rate is not arbitrary because its only acceptable constant value $\bar{Q}$ must *simultaneously* correspond to a critical point of $Q(H, x)$ (stationary condition) and provide the smallest flow rate (physical limitation). It should be noted that such $\bar{Q}$ is not a local minimum for $Q(H, x)$. In fact, function $Q(H, x)$ from equation (5) has, for typical profiles of $p(x)$ and $\tau(x)$ as those in Fig. 3, two critical points (H_c, x_c) that guarantee the stationary condition

$$\nabla Q(H_c, x_c) = 0.$$

As shown in Fig. 4, one of them is the maximum of surface $Q(H, x)$ ($Q_M = Q(H_M, x_M)$) and the other one is a saddle point ($Q_S = Q(H_S, x_S)$). Since $Q_S < Q_M$, the correct value of the flow rate is $\bar{Q} = Q(H_S, x_S)$. Alternatively, the

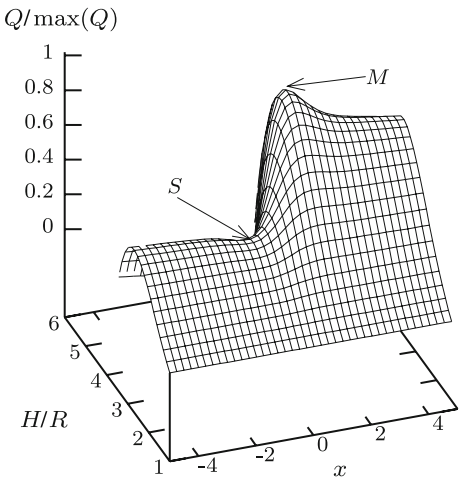

Fig. 4 Surface $Q(H, x)$ (normalized by its maximum) from equation (5) obtained with the pressure and shear stress profiles reported in Fig. 3. S denotes the saddle point, M the maximum. The only physically acceptable value of the withdrawal flux is $\bar{Q} = Q_S$, at the saddle point

maximum is not acceptable because it provides a level curve $H(x)$ at $Q(H, x) = Q_M$ that degenerates in a single point (for the same reason a minimum would not be acceptable), whereas the level curve at $Q(H, x) = Q_S$ (saddle point) provides the unknown function $H(x)$.

The critical points of Q are found by solving

$$\nabla Q = 0 \quad \Longleftrightarrow \quad \begin{cases} \frac{\partial Q}{\partial H} = 0 \\ \frac{\partial Q}{\partial x} = 0, \end{cases} \tag{6}$$

which is a nonlinear system that includes logarithmic functions and, thus, must be treated numerically. Figure 5 reports the curves $\partial Q/\partial x$ (dashed line) and $\partial Q/\partial H$ (dotted line) on the plane $(H/R, x)$ for the surface $Q(H/R, x)$ shown

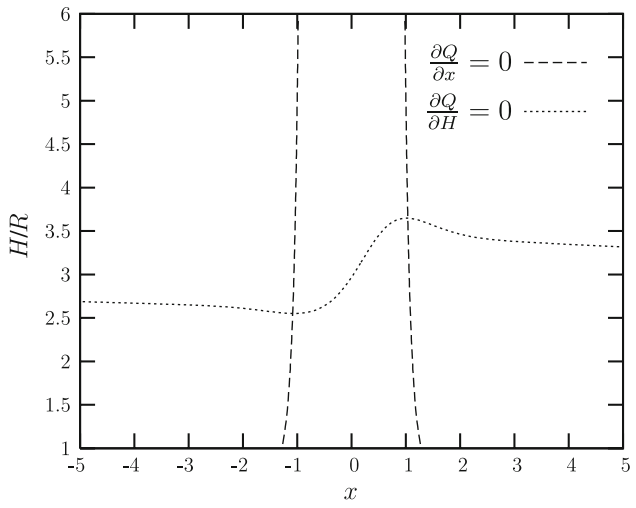

Fig. 5 Graphical solution of system (6) in the plane $(H/R, x)$

in Fig. 4. Condition (6) corresponds, graphically, to the intersection between the curves. The only acceptable solution is the saddle point, on the left.

An easier, but mathematically equivalent, way to compute the saddle point and find $\bar{Q}$ follows two steps: (a) the maximum of the liquid flux $Q_{max}(x)$ is found at fixed x by employing the condition $\partial Q/\partial H = 0$, i.e.

$$UH + \frac{A}{2}H(H^2 - R^2) + \frac{B}{4}(H^2 - R^2) + H^2 \ln\left(\frac{H}{R}\right)\left(\frac{3}{2}B - AH\right) = 0, \tag{7}$$

which provides $H_{opt}(x)$ and then, through equation (5), $Q_{max}(x) = Q(H_{opt}(x), x)$; such a maximum $Q_{max}(x)$ changes with x because so do $H_{opt}(x)$, $p(x)$ and $\tau(x)$; (b) the physically acceptable liquid flux $\bar{Q}$ is the minimum of $Q_{max}(x)$ because, in steady conditions, Q must be constant (continuity equation) and limited by its smallest value. Therefore, we conclude that $\bar{Q} = (Q_{max})_{min}$. This "optimal" approach was used by Elsaadawy et al. (2007), who followed what had already been done by Ellen and Tu (1984). Since it consists in searching for the maximum of $Q(H, x)$ in direction H (at fixed x) and then in searching for the minimum of these maxima in direction x, the "optimal" method is, indeed, equivalent to searching for a saddle point among the critical points of $Q(H, x)$ provided by system (6).

The optimality condition $\partial Q/\partial H = 0$ stated in equation (7) confirms the early result of Deryaguin (1945) who considered the withdrawal of a plate from a liquid bath at high capillary number (i.e. negligible surface tension σ) and concluded that the film thickness is that which results in a maximum volume flux of liquid being entrained by the plate. In other words, the flow adjusts itself until the coating carries as much material as possible. Such optimality condition was recovered also by Homsy and Geyling (1977) in the framework of rapid coating of cylinders without any jet stripping, and further confirmed by Tuck (1983) who analyzed jet stripping on vertical plane surfaces. Tuck (1983) pointed out that experimental evidence (see Deryaguin and Levi 1964; Esmail and Hummel 1975) suggests that Deryaguin's result $\partial Q/\partial H = 0$ is accurate for sufficiently large Capillary number, which is precisely the case of the present work.

It should be noted that, in the special case of no effect of the annular jet, i.e. $dp/dx = 0$ and $\tau = 0$ ($A = \rho g/\mu$ and $B = 0$), equations (3), (5), (7) reduce, respectively, to equations (1), (2), (6) of the theoretical work done by Homsy and Geyling (1977) and carried out under the assumptions of negligible inertial and surface-tension effects.

Once $\bar{Q} = Q_S = (Q_{max})_{min}$ has been found, the mean final thickness is easily determined as

$$h_f = \sqrt{R^2 + \frac{\bar{Q}}{\pi U}} - R. \tag{8}$$

Instead of assuming p and τ as functions of x, an alternative approach—known as "knife" model—considers only what happens at the position $\bar{x}$ where the pressure gradient dp/dx reaches its maximum. The idea is based on the physical observation that the pressure gradient and the wall shear stress reach their respective maximum and minimum more or less at the same position $\bar{x}$, as visible in Fig. 3. Therefore, instead of studying the evolution along x, all quantities are assumed constant and equivalent to their values at $\bar{x}$. Equations (5) and (7) remain formally the same, but now they express two constraints at $\bar{x}$, where H must be replaced by $\bar{H}$, Q by $\bar{Q}$, $dp(x)/dx$ by $dp(\bar{x})/dx = (dp/dx)_{max}$ and $\tau(x)$ by $\tau(\bar{x}) = (\tau)_{min} = -(\tau)_{max}$ (for symmetry reasons). With this notation, $\bar{A}$ and $\bar{B}$ are two constants that depend, respectively, on the maximum pressure gradient and maximum wall shear stress,

$$\bar{A} = \frac{1}{\mu}\left[\left(\frac{dp}{dx}\right)_{max} + \rho g\right], \quad \bar{B} = -\frac{(\tau)_{max}}{\mu}. \tag{9}$$

Once $\bar{H}$ has been determined through (7), $\bar{Q}$ is computed using (5) and, finally, h_f is derived from (8). This model, whose main advantage is that $dp(x)/dx$ and $\tau(x)$ are replaced by two constants, has given encouraging results for jet stripping on a flat surface (Gosset and Buchlin 2007).

The "optimal" and "knife" models are, indeed, very similar and provide comparable results. Among recent works dealing with jet wiping on flat surfaces, the "optimal" approach has been considered only by Elsaadawy et al. (2007), whereas the "knife" approach has been used more extensively (Naphade et al. 2005; Lacanette et al. 2005a, b, 2006; Gosset and Buchlin 2007) because it does not require the complete knowledge of the profiles $p(x)$ and $\tau(x)$.

Regardless of the model employed for predicting the final coating thickness h_f, the most critical issue is the determination of the pressure gradient and wall shear stress (for the "optimal" model) or their maxima (for the "knife" model). The only data known to the author and relative to the geometry in Fig. 1b are those by Anthoine (1996), who provided the correlations

$$\begin{aligned} \left(\frac{dp}{dx}\right)_{max} &= 10\sqrt{2}\frac{P_n}{\sqrt{sZ}} \\ (\tau)_{max} &= 0.083 P_n^{3/4}\left(\frac{Z}{s}\right)^{0.11}, \end{aligned} \tag{10}$$

where P_n is the nozzle stagnation pressure, s is the width of the nozzle slot and $Z = (D - d)/2$ is the distance between the nozzle slot and the wire, with D denoting the nozzle internal diameter and $d = 2R$ the wire diameter (see Fig. 2). The maximum pressure gradient was obtained from pressure measurements on the surface of a small cylinder (tube) set in the center of an annular jet as in Fig. 1b. The correlation for the maximum wall shear stress was obtained from numerical simulations carried out with Fluent® and from some heat-transfer measurements.

3 Experimental measurements of the final thickness and comparisons with different models

Experimental results were obtained using the GALFIN facility originally developed and constructed at the von Kármán Institute (VKI) to carry out measurements during the wire coating process. The wire is typically 8 m long and 2 mm in diameter and forms a closed loop. Its tension is ensured by a mechanical stretching device and a set of pulleys, whereas a motor connected to one of them moves the wire at a constant speed owing to friction. After the wire has gone through the liquid bath (as in Fig. 1a) and the coating characteristics have been detected, it is cleaned by a doctor blade so as to recover the liquid (that goes back to the bath) and to avoid slippery conditions between the driving pulley and the wire, which could compromise the wire speed and, consequently, the measurement. The liquid typically employed for the tests is silicon oil, with the possibility to use different values of viscosity, density and surface tension. The values used for these experiments are reported in Table 1. A complete description of the facility can be found in Zuccher (1999).

The measurement technique was chosen in order to allow the detection of possible waves developing in the coating so as to study the instabilities of the liquid film occurring in the jet stripping process. A new laser-sheet based non-intrusive experimental technique that could satisfy the requirements of both good spatial resolution and high sampling frequency was employed (see Zuccher 2005). As sketched in Fig. 6, a laser source produces a laser sheet 5 mm wide, which is collected by a receiver

Table 1 Typical liquid properties and operating parameters used in the experiments

Description	Symbol	Values	Dimensions
Wire velocity	U	0.25–1.32	m/s
Liquid density	ρ	951	kg/m^3
Liquid viscosity	μ	0.114	kg/(m s)
Liquid surface tension	σ	0.02	kg/s^2
Wire diameter	d	0.002	m
Nozzle internal diameter	D	0.014	m
Nozzle slot	s	0.001	m
Nozzle stagnation pressure	P_n	500–4,000	Pa

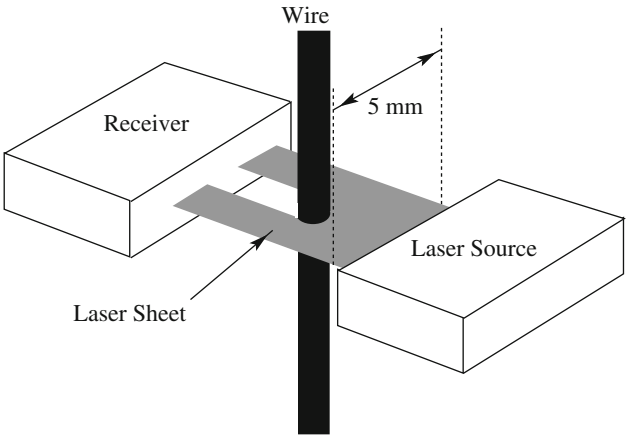

Fig. 6 Sketch of the laser probe. The laser sheet produced by the laser source is detected by the receiver. The wire, covered by the liquid film and positioned in between, interrupts part of the laser, allowing a very precise measurement based on the output signal from the receiver

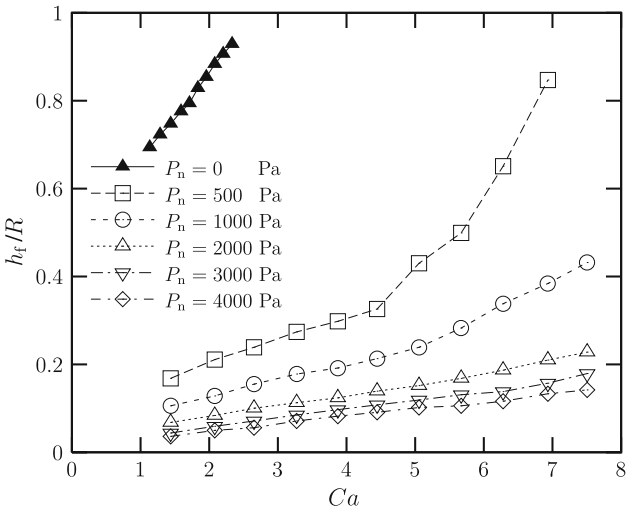

Fig. 7 Normalized mean final thickness as a function of the Capillary number for different values of the nozzle stagnation pressure

placed in front of the source at about 300 mm with the wire positioned in between. The measurement is easily obtained because the light detected by the receiver is linearly proportional (with a negative slope) to the diameter of the wire covered by the coating film. This probe allows a sampling frequency up to 3 kHz with a 5 μm spatial resolution. Moreover, the problem of a wire moving in the horizontal plane is completely overcome because the total light received by the detector does not depend on the position of the wire, which is, thus, free to oscillate within the 5 mm span. A remarkable advantage of such a technique is that the wave speed can be retrieved by using two probes set at a known distance from each other and by performing the cross-correlation between the two signals.

The possibility to extract information on wave characteristics through this technique relies on the assumption of axisymmetric waves. A technique for the detection of non-axisymmetric waves would require multiple probes acting in the same plane perpendicular to the wire but in different azimuthal positions. Due to the complexity of such a system, investigations are here limited to one azimuthal position, assuming axisymmetric waves as done in several theories (see, e.g., Lin and Liu 1975) and models previously mentioned. The voltage from the laser-sheet probe is converted into the total diameter, which includes both the wire and the coating. In order to retrieve the liquid-film thickness $h(t)$ it is necessary to know the mean wire diameter d, which is obtained by averaging the diameter as a function of time measured during a dry run in which the total wire length is scanned for a sufficient number of times. The mean value of the final thickness h_f is eventually retrieved simply by averaging $h(t)$.

Figure 7 reports the normalized mean final thickness h_f/R as a function of the Capillary number $Ca = U\mu/\sigma$ for different values of the nozzle stagnation pressure, whereas Fig. 8 shows h_f/R as a function of the nozzle stagnation pressure for different values of the Capillary number. The distance from the annular jet is $L = 134$ mm; in some preliminary tests (for details see, Zuccher 1999), the mean final thickness was measured at two different distances from the jet, $L = 84$ and 134 mm, respectively, and it was found, within experimental uncertainties, that the measurement was repeatable and that the mean final thickness reached its asymptotic value. Instead of dividing the dimensional thickness h_f by the reference length $h_0 = \sqrt{\mu U/(\rho g)}$, typically used for planar geometries, we normalized h_f with respect to the wire radius R so as to have an immediate idea of the final thickness in terms

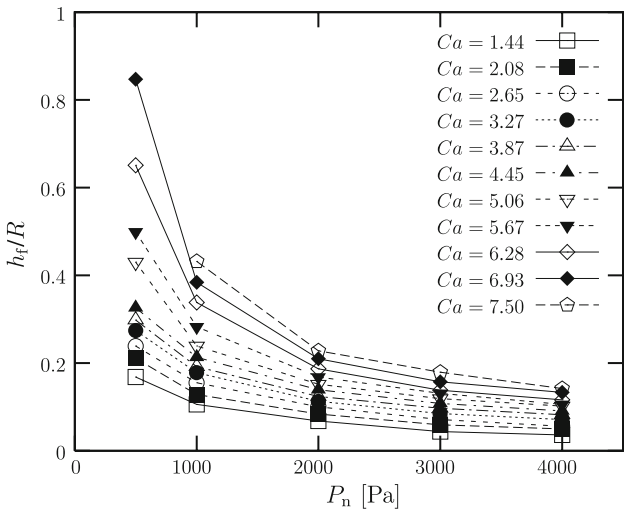

Fig. 8 Normalized mean final thickness as a function of the nozzle stagnation pressure for different values of the Capillary number

of wire dimensions. In Fig. 7 data without jet wiping ($P_n = 0$) have also been reported in order to allow the direct comparison with the dip-coating case (data from Zuccher 2005). Results are as expected. For increasing Capillary number the mean final thickness increases at constant nozzle stagnation pressure, whereas the increase of the stagnation pressure at constant Capillary number leads to a smaller final thickness. While results at high stagnation pressures ($P_n \geq 2{,}000$ Pa) seems to be linearly equispaced as a function of P_n and Ca, for low stagnation pressures ($Pn = 500$ and 1,000 Pa) the mean final thickness grows quite fast with the Capillary number. This is probably the signature of some nonlinear phenomena occurring in that range of operating parameters. It should be noted that for the smallest stagnation pressure and the largest capillary number the mean final thickness is about 85% of the wire radius, i.e. many of the assumptions employed to develop the one-dimensional model in Sect. 2 might not be verified.

In order to compare the experimental results with some theoretical predictions, several different "knife" models are tests (see Table 2). Model M1 refers to the correlations for the maximum pressure gradient and wall shear stress suggested by Anthoine (1996), who specifically studied an annular jet impinging on a small tube (wire). Results are as in Fig. 9. The predicted values are much smaller than the measured ones, meaning that the maximum pressure gradient is overestimated, with relative errors $\epsilon = |h_{f\text{predicted}}/h_{f\text{measured}} - 1|$ between 35 and 85% (the average is $\bar{\epsilon} = 60\%$). This is quite discouraging because such correlations were the only data available in literature for the geometry studied here.

Some reservations on model M1 were expressed in a following project carried out at the von Kármán Institute for Fluid Dynamics (Passelecq 1997), in which 0.72 was suggested as the constant for the correlation of the maximum pressure gradient to replace $10\sqrt{2}$. We refer to this second option as model M2 (see Table 2 for details). Results are shown in Fig. 10. Clearly, the predicted values are now much larger than the experimental ones meaning that the estimated pressure gradient is too week. The relative errors are still very large and have about the same average as model M1.

Model M3 employs the correlations suggested by Elsaadawy et al. (2007), who derived pressure and wall shear stress distributions as a function of the slot gap s and impingement distance Z for a two-dimensional jet impinging

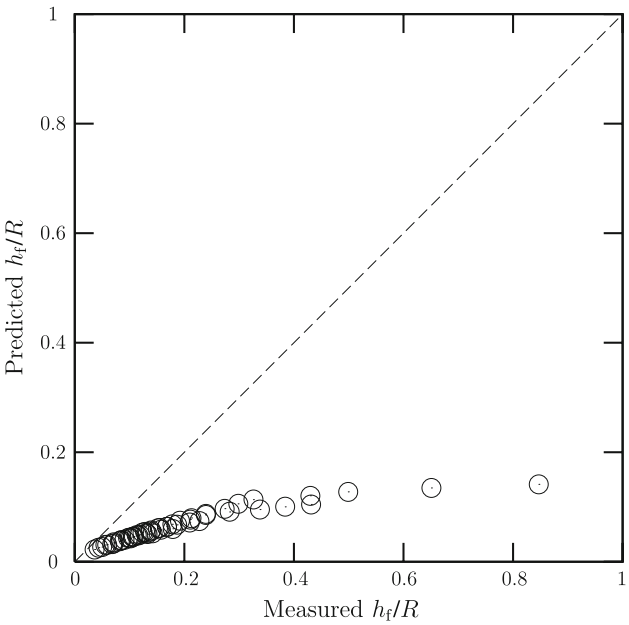

Fig. 9 Comparison between measured and predicted dimensionless mean final thickness h_f/R, knife model M1

Table 2 Summary of knife models employed for comparison with present experiments

Model	$(\mathrm{d}p/\mathrm{d}x)_{\max}$	$(\tau)_{\max}$
M1	$10\sqrt{2}\dfrac{P_n}{\sqrt{sZ}}$;	$0.083\left(\dfrac{Z}{s}\right)^{0.11} P_n^{3/4}$
M2	$0.72\dfrac{P_n}{\sqrt{sZ}}$;	$0.083\left(\dfrac{Z}{s}\right)^{0.11} P_n^{3/4}$
M3	$0.714\dfrac{-0.0056\left(\dfrac{Z}{s}\right)^2 + 0.0268\left(\dfrac{Z}{s}\right) + 1.0108}{s\left[0.0453\left(\dfrac{Z}{s}\right) + 0.7921\right]} P_n$;	$\left[-0.0001\left(\dfrac{Z}{s}\right) + 0.0035\right] P_n$
M4	$0.263 \cdot \left(\dfrac{P_n}{U}\right)^{\frac{0.2}{0.7}} \dfrac{P_n}{\sqrt{sZ}}$;	0
M5	$k(U, P_n) \cdot 0.714\dfrac{-0.0056\left(\dfrac{Z}{s}\right)^2 + 0.0268\left(\dfrac{Z}{s}\right) + 1.0108}{s\left[0.0453\left(\dfrac{Z}{s}\right) + 0.7921\right]} P_n$;	$\left[-0.0001\left(\dfrac{Z}{s}\right) + 0.0035\right] P_n$

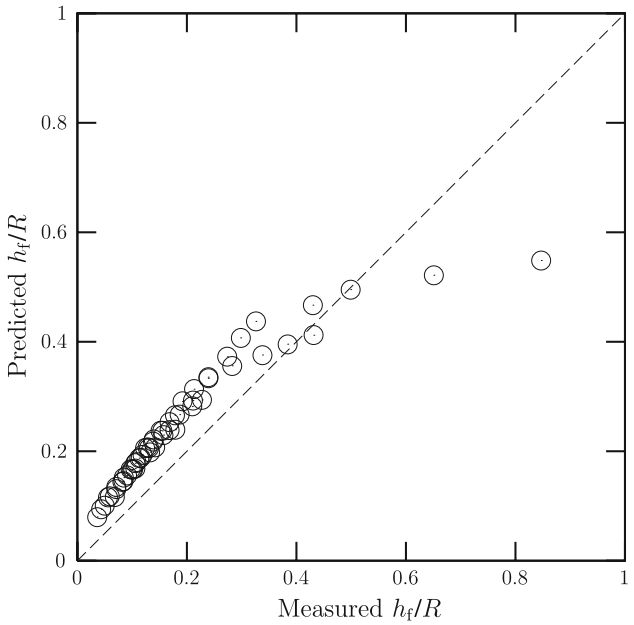

Fig. 10 Comparison between measured and predicted dimensionless mean final thickness h_f/R, knife model M2

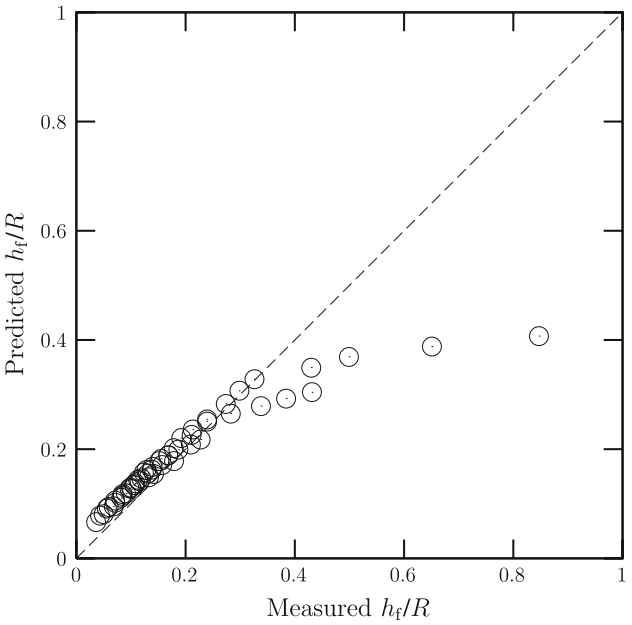

Fig. 11 Comparison between measured and predicted dimensionless mean final thickness h_f/R, knife model M3

on a flat plate in the range $Z/s \leq 8$. The Gaussian shape $p(x) = p_{\max} e^{c\xi^2}$ is typically used for the pressure distribution of an impinging jet, where $p_{\max}$ is the pressure maximum (at the stagnation point), $c = \ln(1/2) \approx -0.693$ and $\xi = x/b$ with b denoting the half width of $p(x)$, i.e. the position x where $p = p_{\max}/2$. Even though Elsaadawy et al. (2007) proposed a slightly different shape of the pressure distribution, they showed that the Gaussian choice provides very good results. Having the analytical form of $p(x)$, the maximum of the pressure gradient is readily found at $x = \pm b/\sqrt{-2c}$, where $|(\mathrm{d}p/\mathrm{d}x)_{\max}| = \sqrt{-2c/\mathrm{e}} \cdot p_{\max}/b$. The correlations by Elsaadawy et al. (2007), valid only in the limit $Z/s \leq 8$,

$$\begin{aligned} \frac{b}{s} &= 0.0453\left(\frac{Z}{s}\right) + 0.7921 \\ \frac{p_{\max}}{P_n} &= -0.0056\left(\frac{Z}{s}\right)^2 + 0.0268\left(\frac{Z}{s}\right) + 1.0108 \\ \frac{\tau_{\max}}{P_n} &= -0.0001\left(\frac{Z}{s}\right) + 0.0035 \end{aligned} \tag{11}$$

can, thus, be inserted into $|(\mathrm{d}p/\mathrm{d}x)_{\max}| = \sqrt{-2c/e} \cdot p_{\max}/b$ and, after noting that $\sqrt{-2c/\mathrm{e}} \approx -0.714$, it is straightforward to obtain the maximum pressure gradient and wall shear stress of model M3 as in Table 2. It should be noted that equations (11) are valid in the range $Z/s \leq 8$, which is precisely our case since in the experiments $Z/s = 6$ ($Z = 0.006$ and $s = 0.001$, see Table 1). By comparing the predicted and measured values of the mean final thickness (see Fig. 11), a quite good agreement is found only for $h_f < 0.4$. This is due to the fact that at low stagnation pressure P_n and high wire speed U, i.e. when h_f is large, phenomena not considered in the simple one-dimensional knife model take place. Many of the initial hypotheses might not be verified because of possible loss of axial symmetry, non-negligible effects of surface tension, strong nonlinearities affecting the advection terms of the Navier–Stokes equations and here disregarded, possible influence of the coating film on the jet characteristics, etc. Despite the fact that circles in Fig. 11 are localized in the vicinity of the diagonal, errors can be easily identified for small values of h_f, leading to quite large relative errors on the order of $\bar{\epsilon} = 25\%$.

Model M4 is based on a very simple attempt to use a modified expression of that proposed by Anthoine (1996) for the maximum pressure gradient, where the constant $10\sqrt{2}$ is replaced by $0.263(P_n/U)^{0.2/0.7}$, i.e. an expression that depends on both P_n and U. The coefficient 0.263 was chosen empirically so as to match the value of h_f at $U = 0.78$ m/s and $P_n = 2{,}000$ Pa. Results are remarkably good, as shown in Fig. 12. As opposed to model M3, now the best agreement is found for small values of h_f, leading to an average relative error $\bar{\epsilon} = 8\%$. However, some discrepancies are still present for very large values of the mean final thickness, $h_f/R > 0.3$, i.e. for the seven points in Fig. 12 which are the most distant from the dashed line. If such points are disregarded, because they might have been obtained in the range of parameters in which many of the initial hypotheses were not verified, the average relative error drops to $\bar{\epsilon} = 5.5\%$.

Model M5 is based on the idea that a reliable expression of the pressure gradient, such as the one proposed by

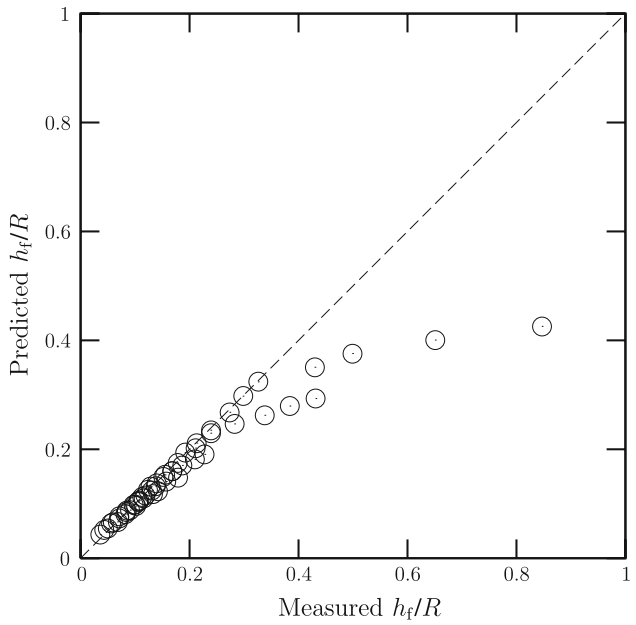

Fig. 12 Comparison between measured and predicted dimensionless mean final thickness h_f/R, knife model M4

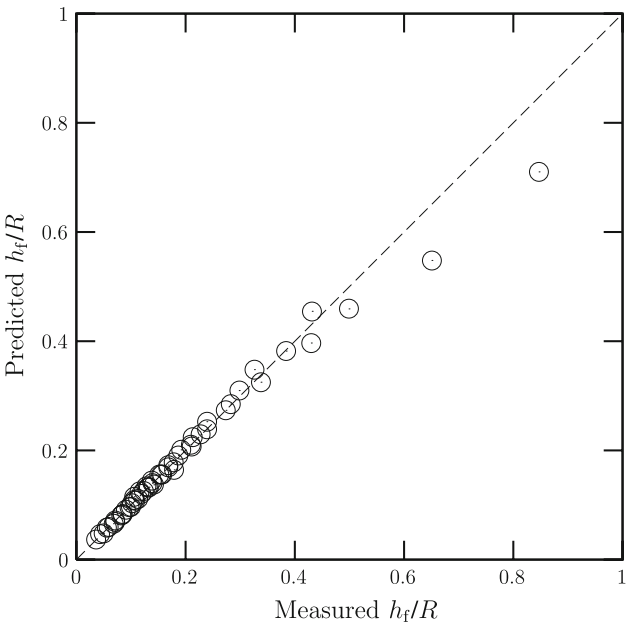

Fig. 13 Comparison between measured and predicted dimensionless mean final thickness h_f/R, model M5

Elsaadawy et al. (2007), could be empirically modified in order to account for the annular geometry and for other unknown phenomena occurring for $h_f \geq 4$. In other words, the expression of the pressure gradient in model M3 is multiplied by a function $k(U, P_n)$ obtained by correlating the coefficients needed to match the predicted and measured values of h_f at a particular U and P_n, as resulting from Fig. 7 or 8. Such a correlation takes the form

$$k(U,P_n) = \sum_{i=1}^{3}\left[\left(\sum_{j=1}^{3} a_{ij}U^{3-j}\right)P_n^{3-i}\right], \qquad (12)$$

with

$$A = \begin{bmatrix} 9.628\times10^{-8} & -2.477\times10^{-7} & 6.474\times10^{-8} \\ 4.227\times10^{-4} & -4.980\times10^{-4} & 6.819\times10^{-4} \\ -9.220\times10^{-1} & 3.161\times10^{-1} & 9.391\times10^{-1} \end{bmatrix}$$

Function $k(U, P_n)$, which can be more easily recognized if expanded as $k(U, P_n) = (a_{11}\,U^2 + a_{12}\,U + a_{13})\,P_n^2 + (a_{21}\,U^2 + a_{22}\,U + a_{23})\,P_n + (a_{31}U^2 + a_{32}U + a_{33})$ is reported in Fig. 14. Results obtained with model M5 are shown in Fig. 13. All measured values are very well captured by the predicted ones, except for the two experiments with the largest h_f which were carried out at the lowest nozzle pressure and highest wire speed. As opposed to all previous models, the average relative error is now very small, $\bar{\epsilon} = 3\%$.

For all models here considered it was found that the major role in the prediction of the mean final thickness h_f is played by the maximum pressure gradient rather than the

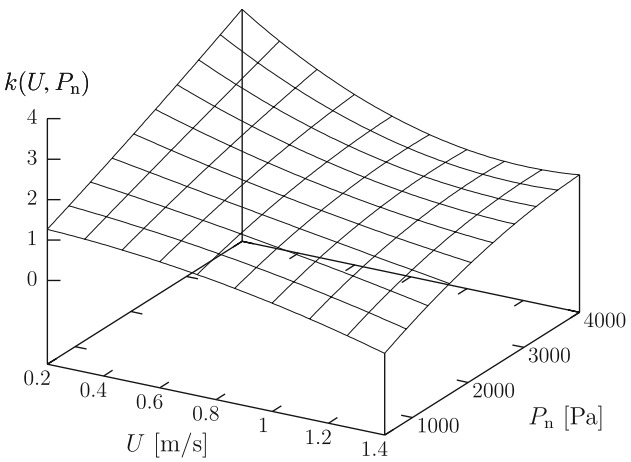

Fig. 14 Function $k(U, P_n)$ used to correct the correlations for two-dimensional jet impinging on a flat plate

maximum shear stress. In a first-approximation model, therefore, the latter can be set to zero.

Knife models are the current state of the art for predicting the mean final thickness in planar jet wiping configurations. However, the fact that surface tension effects are negligible suggests that the run-back flow in the case of annular jet wiping is due to the dynamic pressure of the air jet. The Landau–Levich–Deryaguin (LLD) theory (see Landau and Levich 1942; Deryaguin 1945; Levich 1962; Deryaguin and Levi 1964) generalized for the cylindrical case, $h_f \sim RCa^{2/3}$, can, thus, be rearranged by

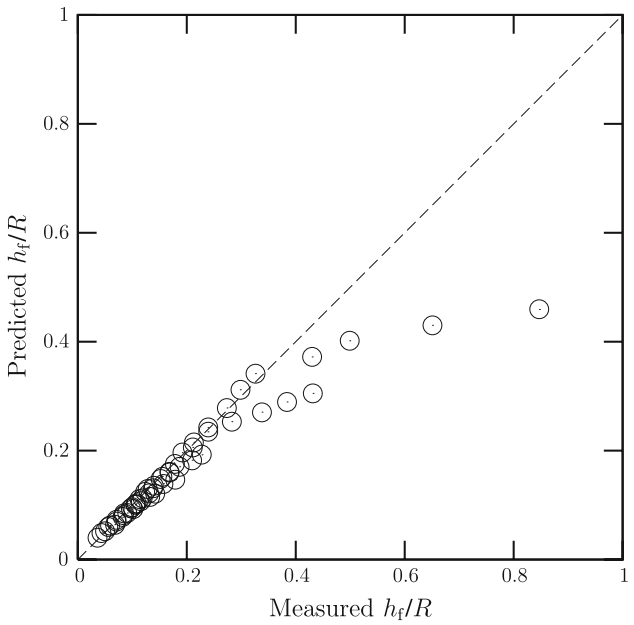

Fig. 15 Comparison between measured and predicted dimensionless mean final thickness h_f/R as from equation (13)

replacing the capillary pressure σ/R with the nozzle pressure P_n. The result is

$$h_f = KR^{1/3}\left(\frac{\mu U}{P_n}\right)^{\frac{2}{3}}, \quad K = 1.08, \tag{13}$$

where the constant K has been determined by minimizing the difference between the experimental final thickness reported in Fig. 8 for $Ca < 4.5$ and the one predicted by equation (13). As shown in Fig. 15, results are quite similar to those provided by model M4, which is, indeed, similar to the simple formula (13) in the sense that in both cases h_f depends on a function of $(U/P_n)^{\alpha}$. The average relative error of the data in Fig. 15 is $\bar{\epsilon} = 8\%$, with some discrepancies visible for very large values of the mean final thickness where model (13) is not valid.

4 Characteristics of the waves developing in the liquid film

The details on how to retrieve wave characteristics using the laser-sheet probe and the appropriate post-processing procedure can be found in Zuccher (2005). The phase speed is measured by utilizing, during the same test, two probes as the one in Fig. 6 and positioned at a distance ΔL from each other. The time delay Δt needed for a particular surface peak to travel from the first probe to the second one is found by performing the cross-correlation between these signals. Having measured the distance ΔL between the two laser sheets, the absolute phase speed is computed as $c_r = \Delta L/\Delta t$.

The wavelength of the perturbation is extracted by employing the Fast Fourier Transform (FFT) of the signal $h(t)$. Since in one time history there might be more than a single peak, the relative importance of each wavelength with respect to the whole signal is measured by the ratio between the integral of the spectrum around the peak and the integral of the entire spectrum. For each of such observed wavelengths, the corresponding amplitude is computed by reconstructing a new signal that contains only the wavelengths in the range of interest. This is done with a band-pass filter or, simply, by multiplying the original spectrum by a unitary shape function different from zero only in the band range and by applying an inverse FFT. Low frequencies are responsible for slow variations of the signal and account for large variations in its amplitude, whereas higher frequencies can be associated either with very small wavelengths or electronic noise and do not contribute considerably to the signal amplitude. The amplitude A is defined as half of the difference between the maximum and the minimum of the wave (half peak-to-peak amplitude) and is computed as $A = \mathrm{std}(h)\sqrt{2}$, where std($h$) is the standard deviation of the filtered signal.

The stable or unstable nature of the liquid film is associated with the growth (or decay) rate. The form of the perturbation is typically $A = A_0 \exp(\mathrm{i}\,(x - ct))$ (see, e.g., Lin and Liu 1975), where A is the amplitude at a certain point x in space (along the wire) and t in time, $c = c_r + \mathrm{i}\,c_i$ is the complex wave speed and x and t are measured with respect to the reference location where the amplitude is A_0. By considering two amplitude measurements A_1 and A_2 at different distances from the nozzle, the experimental growth rate $c_i = (1/\Delta t)\ln(A_2/A_1) = (c_r/\Delta L)\ln(A_2/A_1)$ is immediately computed.

Figure 16 reports the wave speed c_r, normalized with σ/μ, as a function of the capillary number. As mentioned above, measurements were carried out by employing two laser probes set at a distance ΔL from each other. In order to check the possible dependence of c_r on ΔL, two sets of data were collected, for $\Delta L = 40$ and 90 mm. The distance of the bottom probe from the nozzle jet was 57 mm. The wave velocity is quite independent of ΔL and is consistently lower than that computed with the linear theory by Lin and Liu (1975). Such a theory was applied straightforwardly by considering only the behavior of the liquid film after the action of the wiping jet. Theory and experiments agree fairly well for low values of the capillary number. Some differences are visible at large capillary numbers, for which the linear theory is, indeed, not appropriate due to the presence of possible nonlinear effects as seen in Fig. 7 for $P_n \leq 1{,}000$ Pa and $Ca \geq 5$. Figure 17 shows the wavelengths λ normalized with the wire radius R for $P_n = 1{,}000$ Pa. Since multiple waves are found for some capillary numbers, the relative weight of each of them with

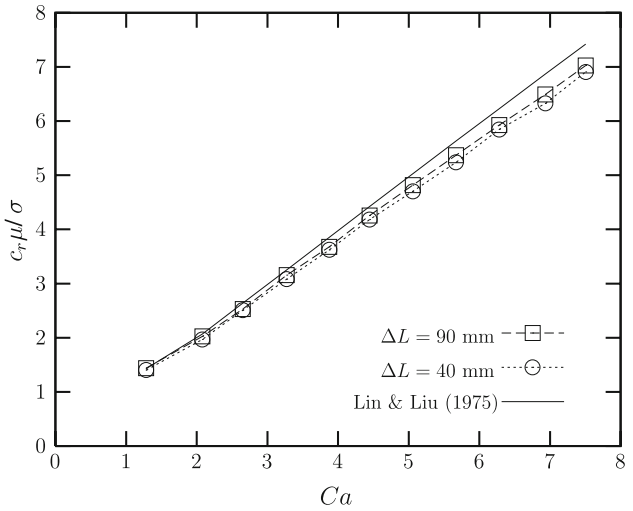

Fig. 16 $P_n = 1{,}000$ Pa. Normalized wave velocity $c_r\,\mu/\sigma$ as a function of the capillary number Ca

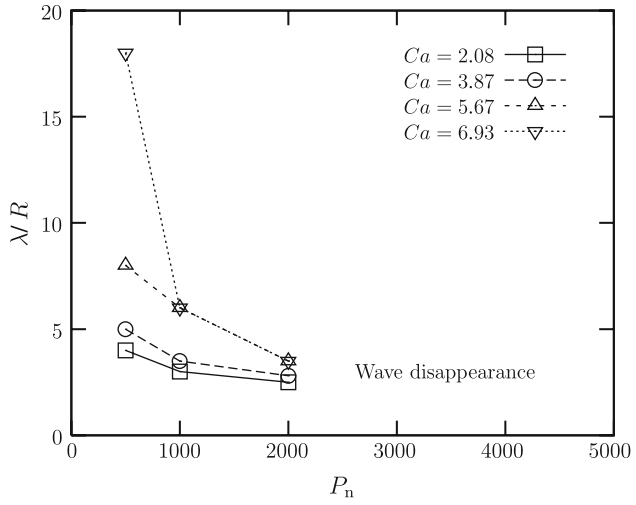

Fig. 18 Normalized wavelength λ/R as a function of the nozzle stagnation pressure P_n for some values of the capillary number Ca

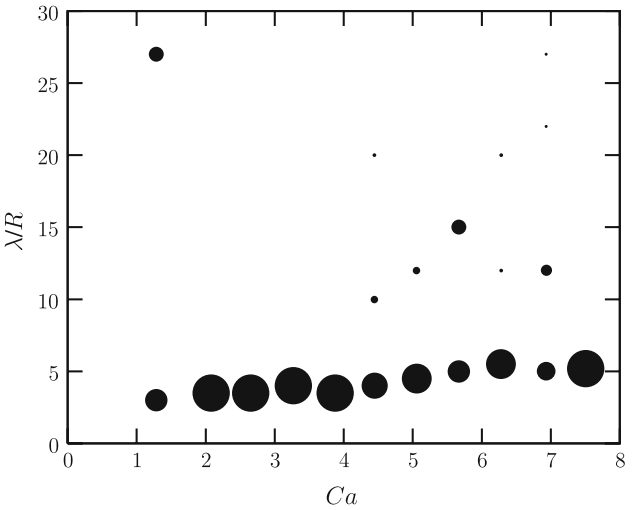

Fig. 17 $P_n = 1{,}000$ Pa. Normalized wavelength λ/R as a function of the capillary number Ca

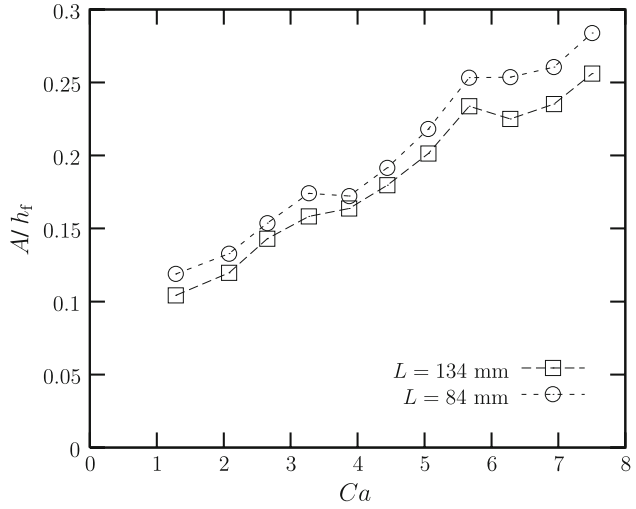

Fig. 19 $P_n = 1{,}000$ Pa. Wave amplitude normalized with mean final thickness h_f as a function of the capillary number Ca

respect to the whole signal is represented by the size of the circles. Multiple waves are typically harmonics, as it is easy to verify, e.g., for the two distinct waves at the lowest stripping speed, whose ratio is 9. The main wavelength slightly increases with the capillary number with a sort of more pronounced step around $Ca = 5$. However, the average wavelength at $P_n = 1{,}000$ Pa is contained within the 3–5 mm range (since $R = 1$ mm, λ/R is the actual wavelength in millimeters).

In order to avoid reporting plots as those in Figs. 16 and 17 for all different values of P_n, the curves in Fig. 18 summarize the behavior of the main wavelength (i.e. the shortest wavelength at fixed Ca and P_n) as a function of P_n for four values of the capillary number. The monotonic decrease of the wavelength λ/R with P_n characterizes all capillary numbers and seems to be quite regular for low values of Ca. The strongest effect is visible at $Ca = 6.93$, probably due to the nonlinear effects occurring when the mean final thickness is large (i.e. at low P_n and high Ca). The most interesting feature of Fig. 18, however, is the disappearance of waves for $P_n > 2{,}000$ Pa, independently of the capillary number. This experimental evidence is quite a remarkable finding. In fact, the mean final thickness h_f can be controlled by changing either the capillary number or the nozzle pressure P_n (see Fig. 7 or 8), but industrial applications require large stripping speeds for productivity reasons together with the absence of waves. From the experiments it seems to be possible to meet both requirements simply by increasing P_n beyond a cut-off value.

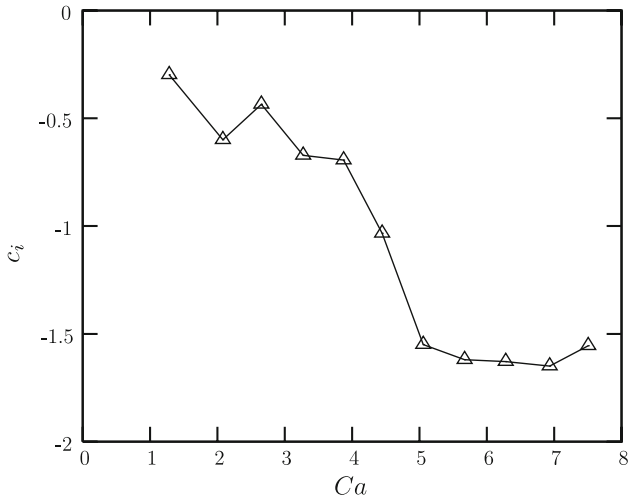

Fig. 20 $P_n = 1{,}000$ Pa. Experimental amplification factor c_i as a function of the capillary number Ca

Figure 19 reports the wave amplitude A normalized with the mean final thickness h_f (instead of R) as a function of the capillary number for $P_n = 1{,}000$ Pa. Since A is quite large and goes from about 10% of h_f for low Ca up to almost 30% for $Ca > 6$, linear theories cannot be used for comparisons. It is interesting to observe that the amplitude detected at the measurement station on the bottom ($L = 84$ mm from the jet nozzle, circles) is always larger than the one at the top ($L = 134$ mm from the jet nozzle, squares), meaning that the perturbations are stable at each capillary number. The very same behavior is found at $P_n = 500$ and 2,000 Pa (figures not reported) and the relative amplitude, at fixed capillary number, decreases with increasing stagnation pressure. Practically speaking, this means that large values of P_n guarantee small relative amplitudes, as one could argue considering that there is a cut-off value of the pressure beyond which no wavelengths can be observed (see Fig. 18).

A quantitative account of the stability of the perturbation is provided by Fig. 20, which reports the experimental amplification factor c_i. As expected from the amplitude plot, the amplification factor is negative and, moreover, the stability of the wave increases with the capillary number.

The experimental finding reported in this section have a remarkable impact on annular jet wiping for industrial applications. Firstly, because the waves, when present, are always stable and therefore their amplitude keeps decreasing as the wire is dragged away from the wiping jet. Secondly, because the stability of the perturbation increases with the production rate (i.e. stripping speed or Ca number), ensuring a better finish of the product in high-productivity conditions. Thirdly, because the amplitude of the waves can be consistently reduced by increasing the nozzle stagnation pressure up to a cut-off value (around 2,000 Pa in these experiments) beyond which no waves can be detected.

5 Concluding remarks

This study presents, for the first time, some experimental investigations carried out to characterize the liquid film left on a wire after it has been withdrawn from a liquid bath and has undergone the action of an annular jet intended to reduce its final thickness. Such a configuration is rather complex and challenging from the theoretical/numerical point of view because it involves the interaction between a turbulent jet and a thin liquid film. Its understanding, however, is particularly interesting for industrial applications such as annular jet wiping.

It is found that the mean final thickness of the liquid film increases with the capillary number (stripping speed) and decreases with increasing nozzle stagnation pressure. Experimental results are compared with an analytical model ("knife" model), which assumes the knowledge of the maximum pressure gradient and maximum wall shear stress due to the jet, and it is based on the liquid properties and operating parameters. The only correlation available for a jet in this geometry leads to very poor results. On the contrary, a correlation recently derived for a two-dimensional jet impinging on a flat plate for the study of planar jet wiping provides a quite good agreement with experimental data. The best comparisons are obtained with modified knife models, which employ a maximum pressure gradient that accounts not only for the nozzle characteristics (stagnation pressure and geometry) but also for the stripping speed. A very simple formula derived from the LLD theory with the capillary pressure replaced by the air-jet pressure provides results comparable to modified knife models.

Since the appearance of surface waves in the final coating sets a limit on the quality of the product, the stability characteristics of the liquid film are also investigated as a function of the capillary number and nozzle stagnation pressure. It is found that typical wavelengths are on the same order of magnitude as the wire diameter and that both, the wavelength and the wave amplitude, decrease for increasing stagnation pressure up to a complete disappearance of waves for a certain cut-off pressure. When waves are detected, the experimental amplification factor is always negative, ensuring a stable film; this feature is enhanced by increasing the capillary number.

References

Alekseenko SV, Nakoryakov VE, Pokusaev BG (1994) Wave flow of liquid films. Begell House, New York

Anthoine J (1996) Annular jet wiping. Project report 1996-02, von Kármán Institute for Fluid Dynamics

Ashforth-Frost S, Rüdel U (2002) Thermal and hydrodynamic visualisation of a water jet impinging on a flat surface using microencapsulated liquid crystals. Int J Fluid Dyn 7:1–7

Chan TL, Leung CW, Jambunathan K, Ashforth-Frost S, Zhou Y, Liu MH (2002) Heat transfer characteristics of a slot jet impinging on a semi-circular convex surface. Int J Heat Mass Transf 45:993–1006

Chen F, Tsaur JY, Durst F, Das SK (2003) On the axisymmetry of annular jet instabilities. J Fluid Mech 488:355–367

Del Taglia C, Blum L, Gass J, Ventikos Y, Poulikakos D (2004) Numerical and experimental investigation of an annular jet flow with large blockage. J Fluids Eng 126:375–384

Deryaguin BV (1945) On the thickness of the liquid film adhering to the walls of a vessel after emptying. Acta Physicochimica URSS 20:349–352

Deryaguin BV, Levi SM (1964) Film coating theory. Focal Point Press, New York

Ellen CH, Tu CV (1984) An analysis of jet stripping of liquid coatings. J Fluids Eng 106:399–413

Ellen CH, Tu CV (1985) Jet stripping of molten metallic coatings. Phys Fluids 28(4):1202–1203

Elsaadawy EA, Hanumanth GS, Balthazaar AKS, McDermid JR, Hrymak AN, Forbes JF (2007) Coating weight model for the continuous hot-dip galvanizing process. Metall Mater Trans B 38B:413–424

Esirgemez E, Newby J, Nott C, Ölcmen S, Ötügen V (2007) Experimental study of a round jet impinging on a convex cylinder. Meas Sci Technol 18:1800–1810

Esmail NM, Hummel RL (1975) Nonlinear theory of free coating onto a vertical surface. AIChE J 21:958–965

Gosset A, Buchlin JM (2007) Jet wiping in hot-dip galvanization. J Fluids Eng 129:466–475

Hewitt GF (1978) Measurement of two phase flow parameters. Academic Press, London

Homsy GM, Geyling FT (1977) A note on instabilities in rapid coating cylinders. AIChE J 23(4):587–590

Lacanette D, Vincent S, Arquis E, Gardin P (2005a) A numerical experiment on the interaction between a film and a turbulent jet. C R Mecanique 333:343–349

Lacanette D, Vincent S, Arquis E, Gardin P (2005b) Numerical simulation for gas jet wiping in steel strip galvanizing process. ISIJ Int 45(2):214–220

Lacanette D, Gosset A, Vincent S, Buchlin JM, Arquis E, Gardin P (2006) Macroscopic analysis of gas-jet wiping: numerical simulation and experimental approach. Phys Fluids 18:042,103

Landau LD, Levich VG (1942) Dragging of a liquid by a moving plate. Acta Physicochim USSR 17:42–54

Levich VC (1962) Physicochemical Hydrodynamics. Prentice Hall, Englewood Cliffs

Lin SP, Liu WC (1975) Instability of film coating of wires and tubes. AIChE J 21(4):775–782

Maurel S, Solliec C (2001) A turbulent plane jet impinging nearby and far from a flat plate. Exp Fluids 31:687–696

Mouza AA, Vlachos NA, Karabelas SVPAJ (2000) Measurement of liquid film thickness using a laser light absorption method. Exp Fluids 28:355–359

Nada SA (2006) Slot/slots air jet impinging cooling of a cylinder for different jets-cylinder configurations. Heat Mass Transfer 43: 135–148

Naphade P, Mukhopadhyay A, Chakrabarti S (2005) Mathematical modelling of jet finishing process for hot-dip zinc coatings on steel strip. ISIJ Int 45(2):209–213

Nozhat WM (1997) Measurement of liquid-film thickness by laser interferometry. Appl Opt 36(30):7864–7869

Olsson EEM, Ahrné LM, Tragårdh A (2005) Flow and heat transfer from multiple slot air jets impinging on circular cylinders. J Food Eng 67:273–280

Passelecq L (1997) Annular jet wiping. Staigiaire report 1997–98, von Kármán Institute for Fluid Dynamics

Patte-Rouland B, Lalizel G, Moreau J, Rouland E (2001) Flow analysis of an annular jet by particle image velocimetry and proper orthogonal decomposition. Meas Sci Technol 12:1404–1412

Pavlova A, Amitay M (2006) Electronic cooling using synthetic jet impingement. ASME J Heat Transfer 128(9):897–907

Phares DJ, Smedley GT, Flagan RC (2000a) The inviscid impingement of a jet with arbitrary velocity profile. Phys Fluids 12(8):2046–2055

Phares DJ, Smedley GT, Flagan RC (2000b) The wall shear stress produced by the normal impingement of a jet on a flat surface. J Fluid Mech 418:351–375

Quéré D (1999) Fluid coating on a fiber. Annu Rev Fluid Mech 31:347–384

Silverman I, Yarin AL, Reznik SN, Arenshtam A, Kijet D, Nagler A (2006) High heat-flux accelerator targets: cooling with liquid metal jet impingement. Int J Heat and Mass Transf 49:2782–2792

Stelter M, Brenn G, Yarin AL, Singh RP, Durst F (2000) Validation and application of a novel elongational device for polymer solutions. J Rheol 44:595–616

Tadmor Z, Gogos CG (1979) Principles of polymer processing. Wiley, New York

Thorton JA, Graff HF (1976) An analytical description of the jet finishing process for hot-dip metallic coating on strip. Metall Trans B 7B:207–218

Tu CV (1995) Impingingement of plane turbulent jets and their application in industrial coating control. Ph.d. thesis, University of Newcastle, Callaghan

Tu CV, Wood DH (1996) Measurements beneath an impinging plane jet. Exp Therm Fluid Sci 13:364–373

Tuck EO (1983) Continuous coating with gravity and jet stripping. Phys Fluids 26:2352–2358

Zuccher S (1999) Liquid film instabilities of wire coatings. Project report 1999-35, von Kármán Institute for Fluid Dynamics

Zuccher S (2005) A novel measurement technique for the study of wire coating instabilities. Exp Fluids 39:694–702

Zuccher S (2008) Experimental investigations of the liquid-film instabilities forming on a wire under the action of a die. Int J Heat Fluid Flow (in press). doi:10.1016/j.ijheatfluidflow.2008.08.004

Zuckerman N, Lior N (2005) Impingement heat transfer: correlations and numerical modeling. ASME J Heat Transfer 127:544–552

Zuckerman N, Lior N (2007) Radial slot jet impingement flow and heat transfer on a cylindrical target. J Thermophys Heat Transfer 21(3):548–561